Soft Matter

PAPER

View Article Online
View Journal | View Issue

Cite this: *Soft Matter*, 2015, **11**, 2018

Ultrasoft, highly deformable microgels

Haylee Bachman,†[a] Ashley C. Brown,†*[a] Kimberly C. Clarke,†[a] Kabir S. Dhada,†[b] Alison Douglas,†[c] Caroline E. Hansen,†[a] Emily Herman,†[a] John S. Hyatt,†[d] Purva Kodlekere,†[a] Zhiyong Meng,†[e] Shalini Saxena,†[f] Mark W. Spears Jr,†[a] Nicole Welsch†[a] and L. Andrew Lyon*[g]

Received 7th January 2015
Accepted 28th January 2015

DOI: 10.1039/c5sm00047e

www.rsc.org/softmatter

Microgels are colloidally stable, hydrogel microparticles that have previously been used in a range of (soft) material applications due to their tunable mechanical and chemical properties. Most commonly, thermo and pH-responsive poly(*N*-isopropylacrylamide) (pNIPAm) microgels can be fabricated by precipitation polymerization in the presence of the co-monomer acrylic acid (AAc). Traditionally pNIPAm microgels are synthesized in the presence of a crosslinking agent, such as *N*,*N*′-methylenebisacrylamide (BIS), however, microgels can also be synthesized under 'crosslinker free' conditions. The resulting particles have extremely low (<0.5%), core-localized crosslinking resulting from rare chain transfer reactions. AFM nanoindentation of these ultralow crosslinked (ULC) particles indicate that they are soft relative to crosslinked microgels, with a Young's modulus of ~10 kPa. Furthermore, ULC microgels are highly deformable as indicated by a high degree of spreading on glass surfaces and the ability to translocate through nanopores significantly smaller than the hydrodynamic diameter of the particles. The size and charge of ULCs can be easily modulated by altering reaction conditions, such as temperature, monomer, surfactant and initiator concentrations, and through the addition of co-monomers. Microgels based on the widely utilized, biocompatible polymer polyethylene glycol (PEG) can also be synthesized under crosslinker free conditions. Due to their softness and deformability, ULC microgels are a unique base material for a wide variety of biomedical applications including biomaterials for drug delivery and regenerative medicine.

Introduction

Microgels are colloidally stable, solvent swollen, hydrogel microparticles with sizes ranging from hundreds of nanometers to tens of microns. Like bulk hydrogels, microgels are mechanically soft, and due to this softness, they exhibit properties that differ significantly from hard spheres. For example, microgels are able to deform and can pass through pores that are much smaller than their own dimensions; resistive pulse analysis of translocation through these pores has previously been utilized to provide information on the details of this deformation.[1,2] Colloidal crystals made from microgels provide unique insights into how soft nanoparticles interact and pack. Microgels can deswell and form assemblies at $\Phi_{eff} > 0.74$, the theoretical limit for hard spheres.[3] This soft particle behavior also allows defect forgiveness in the formation of colloidal crystals that tolerate dopant particles of a different size.[4] Microgel properties, such as size, mechanics and environmental responsivity, are highly tunable through modulation of reaction conditions and monomer, co-monomer and crosslinker identity and concentrations. The very common thermo and pH-responsive poly(*N*-isopropylacrylamide) (pNIPAm) microgels can be synthesized, for example, by precipitation polymerization in the presence of the co-monomer acrylic acid (AAc). Traditionally pNIPAm microgels are synthesized in the presence of a crosslinking agent, such as *N*,*N*′-methylenebisacrylamide (BIS), with the degree of microgel crosslinking influencing microgel swelling and stiffness.[5,6] Microgel crosslinking profoundly modulates individual microgel mechanical properties. Below their lower critical solution temperature (LCST), pNIPAm microgels crosslinked with 2 mol% BIS were found to have a Young's modulus of approximately 80 kPa, compared to 10 mol% BIS crosslinked particles, which were found to have a Young's modulus of approximately 500 kPa.[7] In 2003, Gao and Frisken demonstrated that ultra-low

[a]*School of Chemistry and Biochemistry, Georgia Institute of Technology, Atlanta, GA 30332, USA*

[b]*Department of Biomedical Engineering, University of Texas at Austin, Austin, TX 78712, USA*

[c]*The Wallace H. Coulter Department of Biomedical Engineering, Georgia Institute of Technology, Atlanta, GA 30332, USA*

[d]*School of Physics, Georgia Institute of Technology, Atlanta, GA 30332, USA*

[e]*Entek International LLC, Lebanon, OR 97355, USA*

[f]*School of Materials Science and Engineering, Georgia Institute of Technology, Atlanta, GA 30332, USA*

[g]*Chapman University, Schmid College of Science and Technology, Orange, CA 92866, USA. E-mail: lyon@chapman.edu*

† Equally contributing authors.

crosslinked (ULC) pNIPAm microgels could be synthesized under 'crosslinker free' conditions. These particles are self-crosslinked through a chain transfer reaction at the *tert*-carbon sites which could occur on either the pendent isopropyl group or on the main chain backbone.[8] These chain transfer reactions are rare, and therefore these particles have extremely low (<0.5%) degrees of crosslinking, which appears to be core localized. Previous studies have demonstrated that size and solid density of self-crosslinked pNIPAm microgels can be finely tuned by controlling reaction temperatures, monomer and initiator concentrations.[9] Introduction of comonomers to these ULC microgels was shown to affect particle size, solid density and volume phase transition temperatures.[10] Furthermore, hydrophobic comonomers, such as styrene and methyl methacrylate, were found to decrease particle size and increase solid density, while hydrophilic comonomers, such as acrylic acid (AAc), increased particle size and decreased solid density.[10]

Because crosslinking affects microgel mechanical properties, we hypothesized that ULC microgels would be softer and more deformable than traditionally crosslinked microgels. The presumed softness and high levels of deformability of ULCs make these materials potentially useful for a number of biomedical and tissue engineering applications. Microparticle elastic modulus affects numerous biological responses including *in vivo* dynamics, cellular uptake and extracellular matrix interactions. For example, soft microparticles resembling red blood cells in size have longer circulation times than rigid microparticles of an identical size.[11] Furthermore, hydrogel nanoparticle elasticity has been shown to influence macrophage uptake. Banquy *et al.* recently demonstrated that soft nanoparticles with Young's moduli of ~18 kPa were internalized through macropinocytosis, nanoparticles with Young's moduli between 35 and 130 kPa were internalized *via* clathrin and/or caveolae-mediated endocytosis, and stiff nanoparticles with Young's moduli of ~200 kPa were internalized through clathrin-mediated endocytosis.[12] Additionally, we have recently demonstrated that ULC pNIPAm microgels copolymerized with 5 mol% AAc conjugated to fibrin binding motifs are able to spread within fibrin matrices to a greater extent than BIS crosslinked pNIPAm microgels and induce fibrin matrix collapse, while crosslinked microgels do not induce matrix collapse.[13] The enhanced spreading capability of ULC particles compared to crosslinked particles is presumed to be due to an increased degree of deformability due to the exceedingly low connectivity of ULC microgels. These studies clearly demonstrate the importance of particle softness and deformability in biological applications.

Herein we characterize the deformation of ULC particles compared to traditionally crosslinked particles by AFM analysis of spreading on glass surfaces and the ability to translocate through nanopores significantly smaller than the hydrodynamic diameter of the particles. Furthermore, we characterize softness of ULC particles through AFM nanoindentation. We analyzed deformation of ULC microgels ranging in size from hundreds of nanometers to a few microns in diameter as well as charged and neutral particles to determine if softness and deformability is an overarching feature of microgels synthesized in the absence of crosslinker. A summary of all particles synthesized for these studies can be found in Table 1. Finally, we demonstrate that microgels based on the widely utilized, biocompatible polymer polyethylene glycol (PEG) can also be synthesized under crosslinker free conditions.

Table 1 Summary of synthesis conditions

	NIPAm	AAc	APS	SDS	BIS
ULC	95/90 mol%	5/10 mol%	0.8 mM	—	—
Xlinked	93/88 mol%	5/10 mol%	1 mM	1 mM	2 mol%
NULC-1	100 mol%	—	0.5 mM	—	—
NULC-2	100 mol%	—	8 mM	—	—
SULC-1	100 mol%	5 mol%	1 mM	0.2 mM	—
SULC-2	100 mol%	5 mol%	1 mM	1 mM	—
GULC	90 mol%	10 mol%	2.8 mM	—	—

Experimental

Materials

Chemicals were purchased from Sigma-Aldrich unless otherwise specified. *N*-Isopropylacrylamide (NIPAm) was recrystallized from hexanes (BDH Chemicals). Oligo(ethylene glycol) methyl ether methacrylate (M_n = 300, $OEGMA_{300}$) and poly(ethylene glycol) (200) diacrylate (PEGDA, Polysciences Inc.) were passed through a column of basic Al_2O_3 to remove the inhibitor prior to polymerization. Acrylic acid (AAc, Fluka), *N*,*N*′-methylenebisacrylamide (BIS), sodium dodecyl sulfate (SDS), and ammonium persulfate (APS), and potassium persulfate (KPS), (3-aminopropyl)-trimethoxysilane (APTMS) were used as received. 4-Acrylamidofluorescein (AFA) was synthesized according to a previously published method.[14] Poly(diallyldimethylammonium chloride) (PDADMAC, 400–500 kDa) was diluted with DI water or buffer to a final concentration of 0.1 monoM. Covalent coupling reagents *N*-hydroxysuccinimide (NHS) and *N*-(3-dimethylaminopropyl)-*N*′-ethylcarbodiimide hydrochloride (EDC) were used as received. The following reagents were used to prepare buffers: sodium phosphate monobasic monohydrate, 4-morpholineethanesulfonic acid (MES), *N*-(2-hydroxyethyl)piperazine-*N*′-(2-ethanesulfonicacid) (HEPES), sodium chloride and sodium hydroxide. All water was distilled and deionized (Barnstead E-Pure) to a resistance of 18 MΩ. Additional particulate matter was removed using a 0.2 μm filter.

pNIPAm microgel synthesis

A solution of NIPAm, BIS (for crosslinked particles), and SDS (for SULC particles) dissolved in DI water was filtered into a 3-neck round bottom flask through a 0.2 μm or 0.8 μm Acrodisc syringe filter. In some syntheses, AFA dissolved in DMSO was added to the monomer solution. The round bottom flask was fitted with a condenser, N_2 inlet, and thermometer and charged with the remaining amount of DI H_2O needed. The solution was stirred at 500 rpm (400 rpm for NULCs), purged with N_2, and heated to 70 °C in an oil bath until the temperature was stable

for NULCs and for 1 hour for other ULCs. In the synthesis of anionic microgels, acrylic acid was added to the flask 10 minutes before initiation. Total monomer concentration for ULC, crosslinked, NULC, and SULC microgels was 100 mM while 146 mM total monomer concentration was used for GULC microgels. APS filtered through a 0.2 μm Acrodisc syringe filter was injected into the flask to initiate polymerization, and the reaction was allowed to proceed overnight (4 h for NULCs) under reflux. For GULCs, the reaction was initiated at 45 °C followed by an increase in temperature to 60 °C at a rate of 30 °C h^{-1}. After completion, the reaction solution was cooled to room temperature and filtered through glass wool. Microgels were centrifugally pelleted and redispersed in DI H_2O 3–6 times to purify and then lyophilized before use. The conversion of ULC microgels is approximately 75%.

PEG microgel synthesis

Self-crosslinked PEG-sidechain microgels were synthesized *via* surfactant-free precipitation polymerization in a 250 mL three-necked round bottom flask equipped with a reflux condenser, N_2 inlet, thermometer, and magnetic stirrer. $OEGMA_{300}$ (98 mol%; 80.7 mM final concentration) was dissolved into 84 mL DI H_2O and the solution was degassed at room temperature by flushing with nitrogen for 20 min while stirring. In the next step, the solution was heated to 80 °C in an oil bath and purged with N_2 while stirring at 450 rpm. Methacrylic acid (2 mol%; 1.6 mM final concentration) dissolved in 0.5 mL DI H_2O was added to the reaction solution and stirred for another 10 minutes. The reaction was started by addition of the initiator KPS (0.01 g dissolved in 1 mL DI H_2O; 0.4 mM final concentration). The polymerization was allowed to proceed for 6 hours at 80 °C under a nitrogen blanket. The reaction solution was cooled to room temperature using an ice bath and filtered through glass wool afterwards to remove traces of coagulum. 5 mol% PEGDA crosslinked microgels were prepared analogous to crosslinker-free microgels, but with slightly modified concentrations (93 mol% $OEGMA_{300}$, 76.6 mM final concentration, 5 mol% PEGDA, 4.2 mM final concentration, and 2 mol% methacrylic acid, 1.6 mM final concentration). The final microgels were purified by dialysis (MWCO, 12–14 000 Da) against DI H_2O for two weeks and were lyophilized before use. The conversion of self-crosslinked PEG microgels is approximately 80%.

Microgel size characterization

Microgel size was characterized through AFM imaging, dynamic light scattering (DLS) and pore translocation. Hydrodynamic radii were obtained from DLS measurements (Wyatt Protein Solutions). Samples were analyzed in 25 mM HEPES, 150 mM NaCl buffer at pH 7.4. NULCs were analyzed in 10 mM HEPES, 150 mM NaCl buffer at pH 7. At least 3 sets of 25 acquisitions were used for analysis. Pore translocation of samples in 25 mM HEPES buffer, 150 mM NaCl was analyzed through tunable resistive pulse analysis with a qNano (Izon Science, Oxford, UK). An Asylum Research MFP-3D AFM was used to analyze microgel spreading on APTMS functionalized glass surfaces.[15,16] Silicon nitride cantilevers ($k = 42$ N m^{-1}, NanoWorld) were operated in air using intermittent contact mode. In-liquid AFM images were collected in HEPES or PBS buffer using silicon nitride cantilevers ($k = 0.09$ N m^{-1}). Cantilevers were actuated *via* the Asylum iDrive system operating in intermittent contact mode. All data was processed through software written in the IgorPro environment (Wavemetrics, Inc.).

Viscometry

An Ubbelodhe viscometer was used to measure the time it takes for dilute suspensions of various microgel weight percentages to travel through a capillary. Temperature was controlled by immersing the viscometer in a water bath for the duration of the measurements. The time read out, constant for the viscometer, and density of the solvent was used to calculate the dynamic viscosity of the suspensions. The data were fit to the Einstein–Batchelor equation ($\eta/\eta_0 = 5.9\Phi^2 + 2.5\Phi + 1$) and plotted as the ratio of dynamic viscosity measured to that of the solvent, η/η_0, *vs.* the microgel weight percent (Fig. 1C), to solve for Φ.[17] We note that Φ is proportional to the microgel concentration c, $\Phi = kc$, where the constant k can depend on pH, salt concentration and temperature, for a given microgel, since these variables can potentially affect the particle size. The variables k and η can also be used to understand how the solvent quality affects the solvation/swelling of the particles.

Light scattering

To perform the static and dynamic light scattering measurements (SLS and DLS, respectively) for 5 mol% AAc ULC and 2 mol% BIS crosslinked particles, we used a 3D cross-correlation setup from LS Instruments, where laser light incident onto the sample is scattered into a detector that can be positioned at different angles to the incident beam. Different angles correspond to different momentum changes q of the scattered light, according to $q = \frac{4\pi n}{\lambda_0}\sin(\theta/2)$, where λ_0 is the wavelength of the light in vacuum and n is the solvent refractive index. In SLS, the average intensity scattered into a particular q is analyzed to provide information about the internal structure of the particles. In our case, the accessible q-range includes the Guinier regime, in which the intensity decays according to $e^{-(qR_g)^{2/3}}$, where R_g is the particles' radius of gyration, defined as $R_g^2 = \frac{\int_0^R dr r^4 \rho(r)}{\int_0^R dr r^2 \rho(r)}$.[18] By fitting this to the observed low-q intensity, we obtain R_g values for our particles at different conditions. If instead of averaging, the time-dependent intensity fluctuations are cross-correlated, we can obtain the electric field cross-correlation function, defined as $g_E(\tau) \propto e^{-Dq^2\tau}$,[19] where τ is the correlation lag time and D is the particles' diffusion coefficient. The hydrodynamic radius of our particles is given by the Stokes–Einstein equation, $R_h = k_B T/6\pi\eta D$, where k_B is the Boltzmann constant, T is the temperature in Kelvin, and η is the solvent viscosity.[18] The ratio R_g/R_h is a measure of the mass distribution inside the particles. For a sphere with homogeneous density, R_g/R_h has the analytical value $\sqrt{3/5}$; for a particle with mass

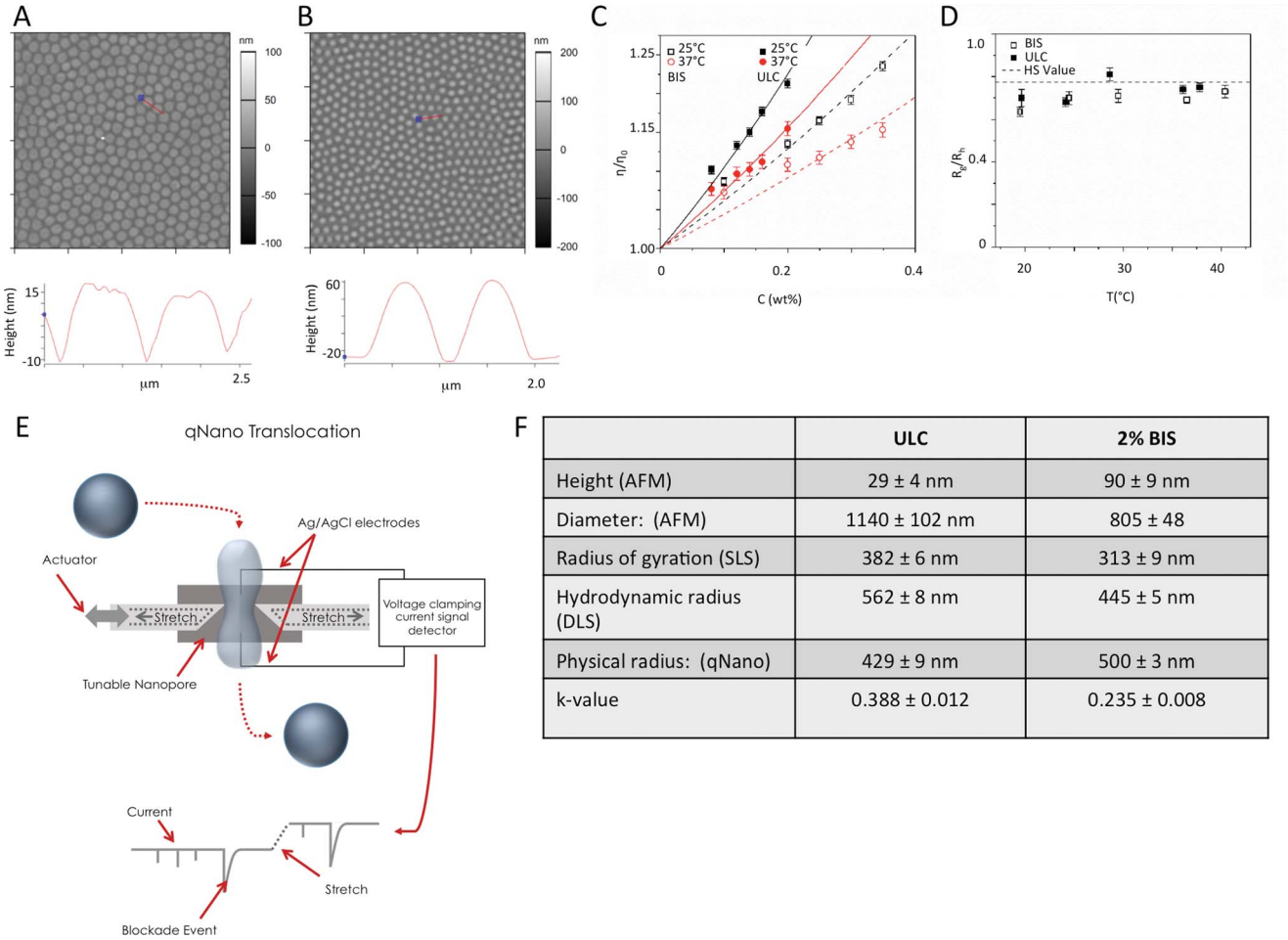

	ULC	2% BIS
Height (AFM)	29 ± 4 nm	90 ± 9 nm
Diameter: (AFM)	1140 ± 102 nm	805 ± 48
Radius of gyration (SLS)	382 ± 6 nm	313 ± 9 nm
Hydrodynamic radius (DLS)	562 ± 8 nm	445 ± 5 nm
Physical radius: (qNano)	429 ± 9 nm	500 ± 3 nm
k-value	0.388 ± 0.012	0.235 ± 0.008

Fig. 1 AFM height traces of dry (pNIPAm-5 mol% AAc) ULCs (A) and 2 mol% BIS crosslinked (pNIPAm-5 mol% AAc) microgels (B) with corresponding height profiles. All height trace images are 20 × 20 µm. Viscometery analysis (C), R_g/R_h measurements from light scattering (D), schematic of qNano size analysis (E) and a summary of particle sizes as determined through AFM, DLS and qNano analysis (F) are presented.

concentrated at the center, such as a core–shell particle, this value is lower, while for a particle with mass concentrated at the outside, such as a hollow sphere, this value is higher. We measure R_g and R_h for our particles over a range of temperatures both above and below the pNIPAm LCST of ~33 °C in pH 7.4 HEPES buffer. Note that although the acrylic acid comonomer is ionized at this pH, which should increase the LCST,[20] its low concentration in the microgels (5 mol%) and screening by the dissolved salt ions should minimize any such LCST perturbation.

Microgel multilayer film fabrication

Lyophilized microgels were redispersed in DI water or PBS overnight on a shaker table. Films were assembled on glass coverslips in accordance with a previously established procedure.[21] Coverslips were cleaned sequentially by sonication in Alconox solution (30 min), DI water, acetone, 95% (v/v) ethanol, and isopropanol (15 min each). Coverslips were subsequently functionalized in a 1% (v/v) 3-aminopropyltrimethoxysilane/absolute ethanol solution for 2 h on a shaker table. Functionalized coverslips were stored in absolute ethanol prior to use. Before microgel deposition, coverslips were rinsed with 95% (v/v) ethanol and DI water, dried with N_2, placed in individual wells of a well plate, and equilibrated in the microgel solvent for 30 min. The solvent was removed and replaced with microgel solution (0.5 mg mL^{-1}). Microgels were centrifugally deposited onto the substrate (2250 × *g*, 10 min, 25 °C). Centrifugal deposition of microgels on substrates facilitates the close packing of microgels on a surface in a reproducible and rapid manner.[21] The coverslips were rinsed copiously with DI water and dried with N_2. This initial layer was covalently coupled to the substrate *via* carbodiimide chemistry. Coverslips were equilibrated in MES buffer (0.01 M, 0.1 mM NaCl, pH 5.3) for 30 min. The buffer was removed and equal volumes of EDC (4 mM in MES) and NHS (10 mM in MES) solutions were added to the wells. The reaction proceeded for 2 h at room temperature on a shaker table. Coverslips were rinsed multiple times with DI water and dried with N_2. Additional microgel layers were added by first adsorbing PDADMAC to the microgel layer to reverse the charge. PDADMAC (1.0 mL, 0.1 monoM in DI water or PBS) was adsorbed for 30 min on the shaker table. The solution was

removed and the coverslips were rinsed extensively with DI water. A second microgel layer was deposited as described above. This process was repeated to yield a 5-layer microgel/4-layer PDADMAC film. AFM imaging was used throughout the film assembly process to monitor surface coverage and film topography.

Microgel deposition on PDMS and stretching

Poly(dimethylsiloxane) (PDMS, Sylgard 184, Dow Corning) was prepared from a 1 : 10 weight ratio of curing agent to elastomeric base. The mixture was cured in a petri dish at 50 °C for 24 h. Cured PDMS was cut to 9×18 mm^2 and placed in hexane for 2 h to remove residual material. The substrates were placed in a vacuum oven overnight at 50 °C to evaporate the solvent. PDMS pieces were stored in DI water prior to surface modification. Hydroxyl groups were introduced onto the surface by incubating PDMS pieces in 1.2 M HCl for 16 h. The substrates were rinsed extensively with water, then absolute ethanol, and were placed in absolute ethanol for 30 min. The PDMS was functionalized in a 1% (v/v) APTMS/absolute ethanol solution for 2 h on a shaker table, and stored in absolute ethanol until used. Following equilibration in PBS, ULCs (0.1 mg mL^{-1} in PBS) were centrifugally deposited onto PDMS at $2250 \times g$ for 10 min. The substrates were subsequently rinsed with DI water and dried with N_2. BIS crosslinked microgels were deposited in an identical manner. After monolayer deposition, the PDMS substrate was loaded onto a homebuilt stretching apparatus[22,23] and imaged *in situ* with a Nanosurf EasyScan 2 AFM at 0% strain (undamaged), 60% strain, and after relaxing back to 0% strain. Si, N-type cantilevers (AppNano, k = 36–90 N m^{-1}) were operated under ambient conditions using intermittent contact mode.

Atomic force microscopy nanoindentation

AFM nanoindentation was performed using an MFP-3D AFM from Asylum Research (Santa Barbara, CA). Samples were prepared by passive deposition or 'active' deposition. Active deposition refers to centrifugal deposition of 1 mL of 1 mg mL^{-1} ULCs suspended in PBS or HEPES buffer for 10 min at $2250 \times g$ onto APTMS functionalized glass coverslips. In contact mode, a 32×32 array of force curves was generated. A conical, silicon nitride tip was used with a spring constant of approximately 0.09 N m^{-1}.

Results and discussion

Size and rheological analysis of ULCs compared to 2 mol% BIS crosslinked particles

ULC microgels were synthesized from pNIPAm and 5 mol% AAc. The size and deformability of ULC particles or 2 mol% BIS crosslinked pNIPAm microgels (also containing 5 mol% AAc) were analyzed through dynamic and static light scattering (DLS/SLS), atomic force microscopy (AFM), pore translocation through resistive pulse analysis (qNano) and viscometry. This array of techniques was utilized to gain a thorough understanding of ULC size, polymer distribution and deformation properties. Results are summarized in Fig. 1. ULC and 2 mol% BIS particles were found to have similar hydrodynamic radii and radii of gyration of 562 ± 8 nm/445 ± 5 nm and 382 ± 6 nm/313 ± 9 nm, respectively. However, ULC particles were found to spread to a much greater extent than crosslinked particles when passively deposited onto a glass surface (Fig. 1). ULC particles were found to have a spread diameter of 1.1 ± 0.1 μm and a height of 29 ± 4 nm compared to crosslinked particles, which were found to have a spread diameter of 0.8 ± 0.5 μm and a height of 90 ± 9 nm. ULC particles, therefore, have a diameter to height ratio that is ~four times larger than that of crosslinked particles, indicating that ULC particles are able to deform more on a surface than similarly sized particles synthesized to contain crosslinker. A summary of size characteristics for all microgels investigated can be found in Table 2.

In many cases, specific properties of suspensions of microgels are dependent on the effective volume fraction occupied by the dispersed component. Volume fraction can also serve as a unifying measure to understand the concentration and phase behavior of a suspension. Thus, we performed viscometric measurements to determine this quantity for both ULC and 2 mol% BIS crosslinked microgel suspensions. Viscometric data were fit using the Einstein–Batchelor equation. From these data, k values were calculated to allow conversion between concentration and volume fraction. It was found that the lowest concentrations of microgels tested deviated systematically from the quadratic fit, which likely represents the sensitivity limits of the viscometer. The fit is constrained to go to one at zero volume fraction, and as a result we find that the deviations in fit at low microgel concentrations have negligible effects on the overall fit. Calculated k values were approximately 1.64 times higher for ULC microgels than 2 mol% BIS crosslinked microgels of similar size. One way to conceptualize this is that 1.64 times more BIS particles by mass must be utilized to reach equivalent volume fractions of ULC particles. This is another demonstration of the low density of these particles compared to more traditionally crosslinked microgels.

To further characterize microgel size and deformability, microgel translocation through pores was analyzed using a qNano instrument (Izon Science). This technique relies on the Coulter principle; resistive-pulse sensing is used to monitor current flow through an adjustable nanopore. Individual particles that pass through the pore create a current differential, resulting in a detected blockade event, and the magnitude and duration of that event is correlated with the size of the particle (Fig. 1E). Sizes of experimental samples are determined by comparing blockade signals to the signals obtained from hard polystyrene beads of known size under identical buffer, pressure and pore size conditions. We hypothesized that due to their deformability, ULC microgels would be able to deform and translocate through pores smaller than their hydrodynamic diameter and would therefore appear smaller than 2 mol% BIS particles using this method. Indeed, ULC microgels were found to have smaller physical radii (429 ± 9 nm) by qNano analysis than 2 mol% BIS crosslinked particles (500 ± 3 nm). In contrast to DLS, dangling polymer chains on the outer shell of a microgel have less of an influence on qNano data. Taken together, these

Table 2 Size characterization summary. NULC values presented are from particles passively deposited into a packed monolayer

	pNIPAM ULC, 5% AAc	pNIPAM, 2% BIS, 5% AAc	NULCs-1	NULCs-2	SULCs-1	SULCs-2	GULCs	PCFs	PEG, 5% PEGDA
Height (AFM)	29 ± 4 nm	90 ± 9 nm	15 ± 2 nm	11 ± 2 nm	10 ± 1 nm	3 ± 1 nm	18.4 ± 4 nm	31 ± 2 nm	137 ± 11 nm
Diameter (AFM)	1140 ± 102 nm	805 ± 48 nm	1230 ± 70 nm	2650 ± 240 nm	1610 ± 210 nm	790 ± 110 nm	7700 ± 900 nm	690 ± 21 nm	827 ± 106 nm
Diameter (DLS)	1124 ± 16 nm	890 ± 10 nm	938 ± 58 nm	1446 ± 96 nm	818 ± 36 nm	422 ± 8 nm	NA	492 ± 9 nm	600 ± 10 nm
Diameter (qNano)	857 ± 17 nm	1000 ± 6 nm	867 ± 182 nm	695 ± 306 nm	327 ± 44 nm	Not detectable	4226 ± 1234 nm	275 ± 8 nm	425 ± 12 nm

data suggest that ULC microgels are less dense than 2 mol% BIS crosslinked microgels, resulting in a smaller qNano size measurement, however, due to the low degree of crosslinking, the polymer chains have enhanced mobility resulting in larger radius measurements than the 2 mol% BIS crosslinked particles when determined *via* light scattering and AFM techniques. Additionally, since these microgels are solvent swollen, they contain a fair amount of the electrolyte in which they are suspended for these measurements. As a result, during microgel translocation events, the change in current detected is lower because of the electrolyte within the microgel, which results in a lower blockage magnitude and a subsequently smaller calculated particle diameter. This effect likely also contributes to the perceived difference in size *via* qNano as compared to DLS data due to the high solvent content and low polymer density.

qNano translocation events are based on the concept that particles can squeeze through a pore that is slightly smaller than the particle diameter. However, success of qNano translocation events is highly dependent on particle deformability in relation to nanopore size. Though pores are adjustable to a certain extent, highly deformable particles present unique challenges to data collection, requiring a small range in pore size for success. When ULC microgels are measured, pores with diameters approximately twice as small as ULC diameters, based on hydrodynamic radius measurements, easily become clogged. In this case, we speculate that ULC microgels are deforming and spreading over the pore, causing pore clogging. In contrast, pores that have a diameter that is similar to ULC microgel diameter present little resistance to these highly deformable microgels, resulting in undetectable translocation events.

Deformation of ULC monolayers

To build upon our characterization of individual ULC microgels, we next sought to characterize deformation of ULC microgel assemblies, by analyzing deformation of ULC monolayers. We have previously demonstrated that multilayer microgel films composed of 2 mol% BIS crosslinked microgels are damaged under applied strain but heal when hydrated.[23] This self-healing behavior was thought to be characteristic only of thick coatings, but here we demonstrate that similar behavior also applies to very thin, single layers of ULCs. A packed monolayer of ULCs was centrifugally deposited onto a functionalized PDMS substrate (Fig. 2A); the PDMS was then elongated by 60% and released so that the substrate returned to its original dimensions. This deformation caused several wrinkles to appear on top of each particle; these wrinkles were aligned and constrained to individual particles (Fig. 2B). When the film was immersed in PBS, the wrinkles were healed and the original monolayer morphology returned (Fig. 2C). No residual effects from the damage/healing process were observed. Microgels of identical chemical composition, but containing 2 mol% BIS crosslinker, were subjected to an identical deposition, stretching, and healing process, however these microgels were not found to individually deform (Fig. 2D–F).

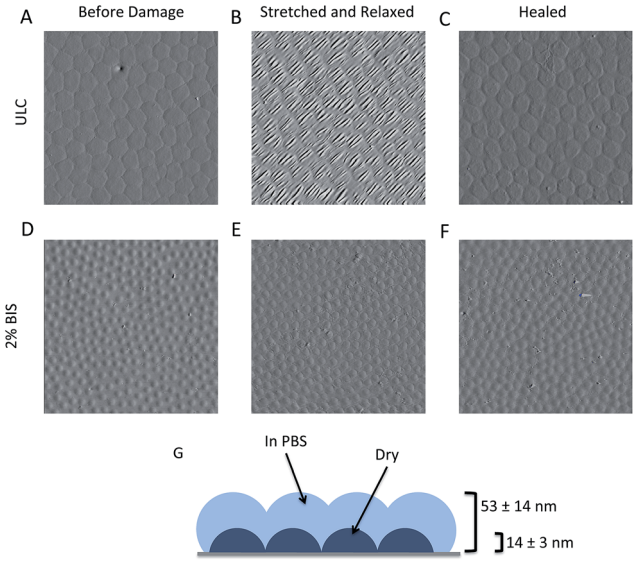

Fig. 2 AFM amplitude images of ULC microgels deposited as a monolayer on PDMS. (A) ULCs have a smooth appearance before linear strain is applied. (B) Wrinkles appear after 60% linear strain is applied and relaxed; wrinkles are confined to each individual particle. (C) Wrinkles heal after exposure to PBS and drying. (D–F) 2 mol% BIS crosslinked microgels do not spread on the PDMS substrate and do not respond to the damage/healing process. (G) Schematic of ULC monolayer swelling behavior in PBS. AFM height traces of scratched monolayers reveal the dry thickness to be 14 ± 3 nm and the swollen thickness to be 53 ± 14 nm ($n = 18$). All AFM images are 20 × 20 μm.

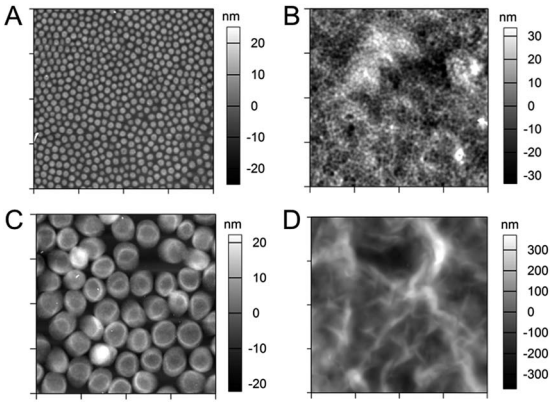

Fig. 3 AFM height retraces of multilayer microgel thin films; 2 mol% BIS crosslinked microgels (A and B) at 1 and 5 layers, respectively, and ULC microgels (C and D) at 1 and 5 layers, respectively. All AFM images are 20 × 20 μm.

Although ULC monolayer deformation/healing contains some similarities to multilayer microgel film deformation/healing, several notable differences exist. In both cases, wrinkles lie along the axis perpendicular to the stretching axis. However, wrinkling of ULCs is representative of buckling of a single particle that is spread on a surface, while wrinkling of multilayer film represents buckling of the film as a whole, with no evidence of individual microgel deformation. ULC monolayers are much more tightly packed than BIS crosslinked microgel monolayers, with no discernable areas of exposed substrate. Swelling upon hydration appears to play a significant role in the healing mechanism in both cases. Multilayers swell by approximately 400%,[23] and ULC monolayers swell by approximately 370% in PBS (Fig. 2G).

These results demonstrate the deformability of ULC particles, even when spread very thin on a surface.

ULC multilayer films

ULC behavior in multilayer films was next analyzed and compared to films constructed from traditionally crosslinked microgels. ULC and 2 mol% BIS crosslinked microgels containing 10 mol% AAc were utilized to construct 5 layer microgel films through active (centrifugal) layer-by-layer (LbL) deposition. ULCs were found to deform substantially during the film fabrication process. As layer number increases, the film takes on a wrinkled texture, where individual, spherical particles can no longer be discerned (Fig. 3C and D); instead, the microgels seem to alter their 3-dimensional shape in response to either the surface topography, complexation with polycation and/or the force applied during deposition. In contrast, 2 mol% BIS crosslinked microgels do not exhibit this same degree of deformation during the fabrication process, and instead retain their spherical shape at higher layer number (Fig. 3A and B). ULC particle deformation suggests that the low degree of crosslinking within the microgel network permits the particles to adopt a variety of shapes within their physical environment.

Neutral ULC microgels (NULCs)

All previous studies were performed with pNIPAm ULC microgels containing AAc (either 5 mol% or 10 mol%). In order to determine if the high level of deformability observed with these anionic microgels was specific to this microgel formulation or applicable to a wide array of formulations, we next synthesized and characterized neutral ULCs (NULCs). NULCs were synthesized in two different size ranges, denoted as NULCs-1 and NULCs-2, by varying initiator concentration while leaving all other synthesis conditions unaltered. NULC size was characterized *via* DLS, AFM and qNano analysis. AFM imaging of NULCs-1 deposited under conditions of active and passive deposition indicated that the microgels spread significantly on the glass surface, with the spreading being most pronounced under conditions of active deposition when the microgels were at sub-monolayer conditions (Fig. 4A–D). While NULCs-2 deposited readily under packed conditions, they could not be deposited as a sub-monolayer, suggesting that microgel–microgel interactions are preferred over microgel–surface interactions. When deposited as a packed monolayer, NULCs-2 were found to have a height of 11 ± 2 nm when deposited through passive deposition and 6 ± 1 nm when deposited through active deposition. Hydrodynamic radii of NULCs-1 and NULCs-2 were 469 ± 29 nm and 723 ± 48 nm, respectively, and radii determined through qNano, were 434 ± 91 nm and 348 ± 153 nm, respectively. The similarities in radii measurements *via* DLS and qNano for NULCs-1 suggest behavior characteristic of less deformable particles. NULCs-2, however, appear to be more

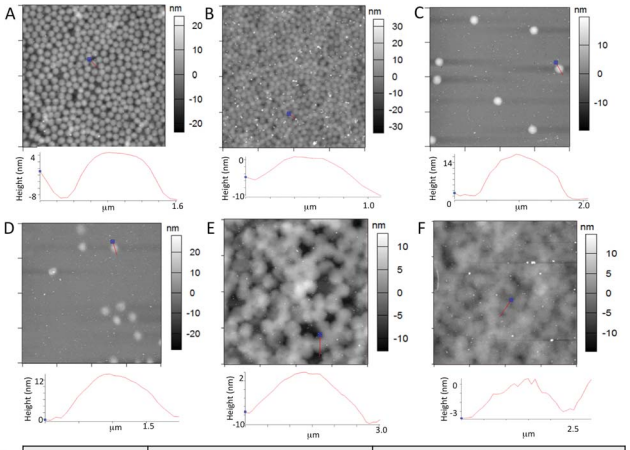

G

	NULCs-1		NULCs-2	
Hydrodynamic Radius (nm): DLS	469 ± 29		723 ± 48	
Diameter (μm): AFM	Passive Deposition	Active Deposition	Passive Deposition	Active Deposition
Sub-monolayer	1.58 ± 0.11	1.91 ± 0.29	N/A	N/A
Packed Monolayer	1.23 ± 0.07	1.06 ± 0.11	2.65 ± 0.24	2.37 ± 0.13
Height (nm): AFM	Passive Deposition	Active Deposition	Passive Deposition	Active Deposition
Sub-monolayer	16 ± 1	13 ± 2	N/A	N/A
Packed Monolayer	15 ± 2	14 ± 3	11 ± 2	6 ± 1

Fig. 4 AFM height traces of Neutral ULCs (NULCs) deposited on APTMS-functionalized glass under different conditions. (A) NULCs-1 deposited by passive deposition for 1 h from a 20 mg mL^{-1} solution. (B) NULCs-1 deposited by active deposition at 2250 × *g* for 30 min from a 0.1 mg mL^{-1} solution. (C) NULCs-1 deposited by passive deposition for 3 h from a 0.1 mg mL^{-1} solution. (D) NULCs-1 deposited by active deposition at 2250 × *g* for 7 min from a 0.1 mg mL^{-1} solution. (E) NULCs-2 deposited by passive deposition for 1 h from a 10 mg mL^{-1} solution. (F) NULCs-2 deposited by active deposition at 2250 × *g* for 1 min from a 0.1 mg mL^{-1} solution. All images are 20 × 20 μm (G) size characterization of NULCs.

deformable, and like anionic ULCs, have physical radii that are considerably smaller than their hydrodynamic radii. While the two types of NULCs behave differently due to differences in their sizes and network structures, they nevertheless demonstrate the deformability that is characteristic of ULCs, albeit to different extents.

Small ULC microgels (SULCs)

In addition to their charge, the size of ULCs can also be modulated. Small ULCs (SULCs) with diameters less than a micron were obtained by performing syntheses in the presence of a surfactant. Modification of the surfactant concentration yielded SULCs of two different sizes: SULCs-1 with a hydrodynamic radius of 409 ± 18 nm and SULCs-2 with a hydrodynamic radius of 211 ± 4 nm. SULCs-1 were found to have a radius of 164 ± 22 nm through qNano analysis, however, SULCs-2 were not detectable with this method, even using the smallest pore size available for the system (~100 nm in diameter). We conclude that due to the small size and deformability of these particles, the smallest pore size available does not hinder translocation of SULCs-2, resulting in undetectable translocation events. AFM imaging on SULCs-1 revealed the presence

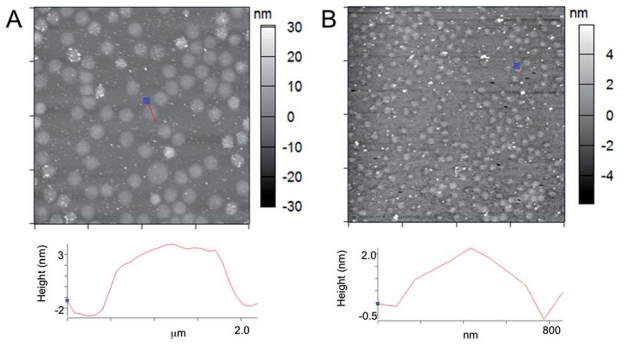

Fig. 5 AFM height traces of Small ULCs (SULCs) deposited on APTMS functionalized glass. (A) SULC-1 deposited by active deposition at 2250 × *g* for 10 min from a 0.0001 mg mL^{-1} solution. (B) SULC-2 deposited by active deposition at 2250 × *g* for 10 min from a 0.001 mg mL^{-1} solution. All images are 20 μm × 20 μm.

of a second, minor population of particles, slightly larger than the SULCs-1 themselves (Fig. 5A). The spreading of both SULCs-1 and SULCs-2 on a flat surface was also observed *via* AFM imaging, and these particles were found to have spread radii of 805 ± 105 nm and 395 ± 55 nm, respectively, and heights of 10 ± 1 nm and 3 ± 1 nm, respectively, which demonstrates the deformability of ULCs even in the size range of the SULCs.

Giant ULC microgels (GULCs)

Conversely, ULC microgels can be synthesized to be multiple microns in diameter. These giant ULCs (GULCs) are synthesized by initiating polymerization at a lower temperature (45 °C) and gradually increasing the reaction temperature to 65 °C.[24] The lower initiation temperature decreases the concentration of radicals in solution, which subsequently decreases the concentration of particle nuclei in solution. Initially, there is a considerably higher monomer to nuclei concentration ratio favoring radical propagation in comparison to initiation, and therefore favoring particle growth over nucleation of new particles. The temperature is gradually increased up to a conventional microgel synthesis temperature to keep the propagation rate high and generate more radicals as monomer is consumed. Like ULCs, GULCs undergo a chain transfer mechanism to produce a self-crosslinked network of low chain density. Thus, GULCs exhibit similar softness and deformability characteristic of ULC particles. Because GULCs are larger in size, their deformability is simpler to qualitatively witness compared to ULCs. The diameter of GULCs in solution was determined by brightfield microscopy to be 3.8 ± 0.4 μm (n = 100) (Fig. 6C). GULCs were found to have a similar diameter (4.2 ± 1.2 μm) through qNano analysis. When deposited in a monolayer at a concentration of 0.01 mg mL^{-1}, particles exhibit an extraordinarily spread diameter of 7.7 ± 0.9 μm and a height of 18 ± 4.0 nm (Fig. 6A). At a slightly higher deposition concentration of 0.05 mg mL^{-1}, the monolayer particle density increases, causing the edges of GULC particles to roll upwards (Fig. 6B). The crowding from neighboring particles limits the available footprint area thereby forcing polymer chain density

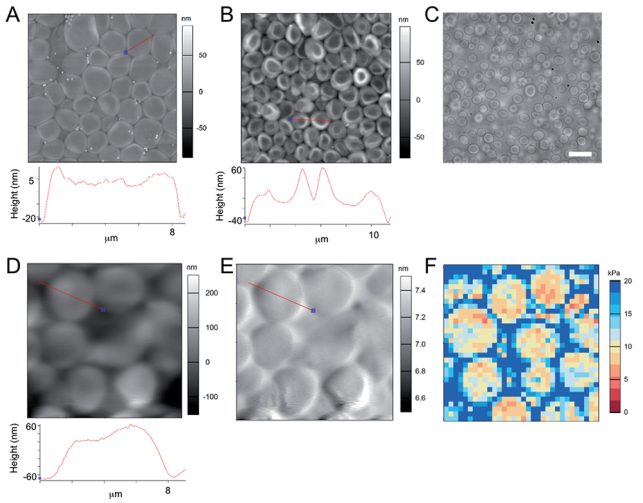

Fig. 6 Giant ULCs (GULC) microgels characterized *via* dry (A and B) and in liquid (D and E) AFM. Height traces (A, B and D) and an amplitude trace (E) of the particles are shown. Brightfield microscopy was used to characterize particle size in solution (C) at 100× magnification (scale bar = 10 μm). AFM nanoindentation (F) was used to determine the elastic modulus. Individual particle height traces are shown directly below each micrograph (A, B and D). AFM images are 40 × 40 μm (A and B) and 20 × 20 μm (D–F).

away from the substrate, resulting in a decrease in footprint to 5.4 ± 0.4 μm, and a height increase to 37 ± 6.7 nm. In-liquid imaging of GULC microgels indicates a height of 100 ± 17 nm (with a spread of 6.9 ± 0.9 μm). It is interesting to note that in hydrated films, individual particles still exhibit noticeable compression from neighboring particles, leading to a non-spherical surface presentation. Because GULC monolayers are much thicker when swollen as compared to smaller ULCs, the Young's moduli of the samples can be found using AFM nanoindentation without significant substrate influence. AFM nanoindentation studies indicated that the elastic modulus of GULCs is approximately 10 kPa, which is more than an order of magnitude smaller than that of traditionally BIS crosslinked microgels[25] under identical buffer conditions. It should be noted that the previous studies used to measure BIS crosslinked samples were in a four layer multilayer assembly, as opposed to a monolayer as in these current studies. Studies conducted in our lab suggest that substrate bleed through may be more significant in the case of smaller microgels, which is why the larger GULC particles were used to obtain elastic moduli measurements in this current study, while thicker multilayers were used in the previous studies. The ability to obtain microgels with elastic moduli in the range of 10 kPa is highly useful for a range of biological applications, particularly for applications seeking to modulate cell fate. Cells are highly sensitive to elastic moduli changes in the range of 0.10 kPa to 100 kPa, depending on the cell type, therefore modulation of this parameter in biomaterials can be used to influence cell fate and function.[26,27] Although GULCs represent a much larger species of the ULC, it is likely that smaller ULC particles exhibit a similar elastic modulus. Thus, ULCs have mechanical properties that are extremely relevant for biological applications.

PEG crosslinker free microgels (PCFs)

We next evaluated whether self-crosslinked microgels could be formed from the widely utilized, biocompatible polymer polyethylene glycol (PEG). Branching and self-crosslinking during free radical polymerization is a well known process for acrylic monomers, such as *N*-vinylformamide, alkyl acrylates and NIPAm, and occurs *via* formation of mid-chain radicals on the polymer backbone.[8,9,28–30] These species are generally formed through hydrogen atom abstraction events yielding *tert*-C free radicals that are stabilized by their conjugation to adjacent groups. In addition to hydrogen transfer originating from the polymer backbone, side-chain transfer products need to be considered as well.[29] In the case of methacrylates, *e.g.* OEGMA, radical chain transfer reactions take place most likely on the highly functionalized side chains.[30] Hydrogen abstraction events result in additional free radicals on the growing polymer

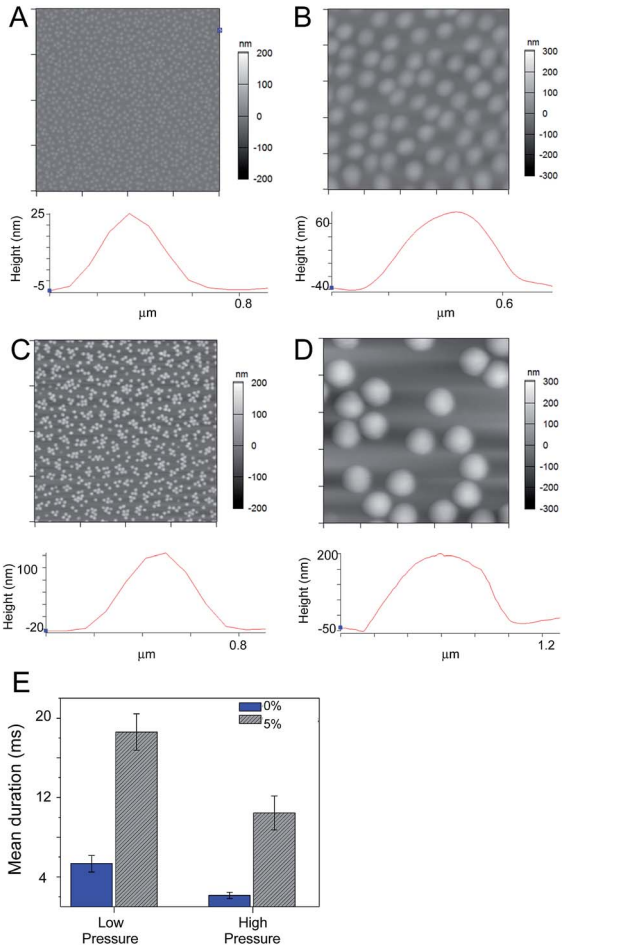

Fig. 7 AFM height retraces of self-crosslinked (A and B) and 5 mol% PEGDA crosslinked (C and D) OEGMA-microgels deposited at 0.25 mg mL^{-1} in 25 mM HEPES/150 mM NaCl pH 7.4 imaged (A and C) after drying and (B and D) after rehydration in buffer. AFM height profiles are shown for the corresponding images. Panel (E) shows the mean blockage duration of self-crosslinked microgels and 5 mol% PEGDA crosslinked microgels during the passage through a nanopore of similar size at low (~300 Pa) and high (~2 kPa) applied pressure. AFM images are 20 × 20 μm (A and C) and 5 × 5 μm (B and D).

chain, *i.e.* in possible crosslinking points, yielding branched and crosslinked microgels with high stability. When using OEGMA as the main monomer for microgel synthesis, the final crosslinking density within the microgel will depend on the length of the ethylene glycol side chains. Self-crosslinked microgels were polymerized from $OEGMA_{300}$, which contains four to five repeating units of ethylene glycol. Thus, eight to ten possible sites per monomer unit exist at which reactive hydrogen atoms can be attacked by free radicals. For stochastic reasons therefore, OEGMA-based microgels likely contain more crosslinking sites than NIPAm-based microgels. As with pNIPAM microgels, spreading of PEG based crosslinker-free microgels was analyzed through AFM imaging and was compared to spreading of 5 mol% PEGDA crosslinked microgels (Fig. 7A and C). Crosslinker-free microgels were found to spread significantly on the glass surface, with a spread diameter of 690 $\pm$ 21 nm and a height of 31 $\pm$ 2 nm, suggesting high particle deformability. In comparison, 5 mol% PEGDA crosslinked microgels were found to have a spread diameter of 827 $\pm$ 106 nm and a height of 137 $\pm$ 11 nm. Upon rehydration, both particle types swell by a factor of 2, but remain spread on the surface (Fig. 7B and D). The deformation of crosslinker-free OEGMA microgels is less pronounced than for pNIPAM ULC microgels, which suggests a higher crosslinking density of the former due to more frequently occurring branching events. Deformability and crosslinking density are also key parameters for the passage of hydrogel particles through nanopores that are of similar or smaller size than the particle dimensions (Fig. 7E). Both at low and high external pressure, crosslinker-free, *i.e.*, more flexible microgels, can pass through the nanopore faster than the stiffer 5 mol% PEGDA crosslinked particles. The differences in translocation time might be of importance for particle clearance from the body by renal filtration.

Conclusions

Herein we have demonstrated that self-crosslinked ULC microgels exhibit unique behaviors compared to crosslinked microgels. Viscometry studies indicate that ULC microgels swell to a greater extent than 2 mol% BIS microgels. AFM characterization of ULC microgels indicates they are highly deformable, spreading over a large area. When deposited on an elastomeric substrate and subjected to a strain, ULC microgels individually deform exhibiting a clear wrinkled pattern, but still maintain self-healing properties when exposed to moisture. ULC microgels containing acrylic acid can be used to build layer-by-layer polyelectrolyte films that exhibit a unique wrinkled topography that varies significantly from films fabricated from 2 mol% BIS microgels. ULC microgels can also be synthesized sans acrylic acid, resulting in neutral ULC microgels. These NULCs exhibit enhanced deformation when actively deposited as compared to passive deposition. Varying synthesis conditions result in ULC microgels of a variety of sizes including SULCs and GULCs. AFM nanoindentation studies indicate that the Young's modulus of GULCs is approximately 10 kPa. Crosslinker free microgels can also be formed using OEGMA; however they do not exhibit the same degree of deformability as pNIPAm ULC microgels. Taken together, these results indicate that ULC microgels possess characteristics that make these particles a unique synthetic microgel candidate for a variety of biomedical applications. Deformability appears to result in ULCs taking on the shape of their underlying surface. Therefore, it is important to keep in mind that although the mechanical properties may be suitable for biomedical materials, the deformability may result in unpredictable structures if not well controlled. On the contrary, if controlled, ULCs could be utilized to obtain assemblies with well-defined shapes for applications such as tissue engineering scaffolds. This deformation could have a number of implications in the application of such materials (*e.g.* drug delivery, biomaterial coatings).

Acknowledgements

Funding sources: American Heart Association Postdoctoral Fellowship to ACB, German Research Foundation (DFG, WE 5485/1-1) Research Fellowship to NW, Georgia Tech President's Undergraduate Research Award to KD, NSF Integrative Graduate Education and Research Traineeship program in Stem Cell Biomanufacturing (0965945) to SS, NSF (2736B48) (SS), American Heart Association Predoctoral Fellowship to AMD.

Notes and references

1 G. R. Hendrickson and L. A. Lyon, *Angew. Chem., Int. Ed.*, 2010, **49**, 2193–2197.
2 D. A. Holden, G. Hendrickson, L. A. Lyon and H. S. White, *J. Phys. Chem. C*, 2011, **115**, 2999–3004.
3 L. A. Lyon, J. D. Debord, S. B. Debord, C. D. Jones, J. G. McGrath and M. J. Serpe, *J. Phys. Chem. B*, 2004, **108**, 19099–19108.
4 A. S. Iyer and L. A. Lyon, *Angew. Chem., Int. Ed.*, 2009, **48**, 4562–4566.
5 B. Sierra-Martin, Y. Choi, M. S. Romero-Cano, T. Cosgrove, B. Vincent and A. Fernandez-Barbero, *Macromolecules*, 2005, **38**, 10782–10787.
6 I. Varga, T. Gilanyi, R. Meszaros, G. Filipcsei and M. Zrinyi, *J. Phys. Chem. B*, 2001, **105**, 9071–9076.
7 A. Burmistrova, M. Richter, C. Uzum and R. von Klitzing, *Colloid Polym. Sci.*, 2011, **289**, 613–624.
8 J. Gao and B. J. Frisken, *Langmuir*, 2003, **19**, 5212–5216.
9 J. Gao and B. J. Frisken, *Langmuir*, 2003, **19**, 5217–5222.
10 J. Gao and B. J. Frisken, *Langmuir*, 2005, **21**, 545–551.
11 T. J. Merkel, S. W. Jones, K. P. Herlihy, F. R. Kersey, A. R. Shields, M. Napier, J. C. Luft, H. L. Wu, W. C. Zamboni, A. Z. Wang, J. E. Bear and J. M. DeSimone, *Proc. Natl. Acad. Sci. U. S. A.*, 2011, **108**, 586–591.
12 X. Banquy, F. Suarez, A. Argaw, J. M. Rabanel, P. Grutter, J. F. Bouchard, P. Hildgen and S. Giasson, *Soft Matter*, 2009, **5**, 3984–3991.
13 A. C. Brown, S. E. Stabenfeldt, B. Ahn, R. T. Hannan, K. S. Dhada, E. S. Herman, V. Stefanelli, N. Guzzetta, A. Alexeev, W. A. Lam, L. A. Lyon and T. H. Barker, *Nat. Mater.*, 2014, **13**, 1108–1114.

14 M. J. Serpe, C. D. Jones and L. A. Lyon, *Langmuir*, 2003, **19**, 8759–8764.
15 K. C. Clarke and L. A. Lyon, *Langmuir*, 2013, **29**, 12852–12857.
16 X. B. Hu, Z. Tong and L. A. Lyon, *Macromol. Rapid Commun.*, 2011, **32**, 1461–1466.
17 B. H. Tan and K. C. Tam, *Adv. Colloid Interface Sci.*, 2008, **136**, 25–44.
18 J. K. G. Dhont, *An Introduction to Dynamics of Colloids*, Elsevier, 1996.
19 K. Schatzel, *J. Mod. Opt.*, 1991, **38**, 1849–1865.
20 K. Kratz, T. Hellweg and W. Eimer, *Colloids Surf., A*, 2000, **170**, 137–149.
21 A. B. South, R. E. Whitmire, A. J. Garcia and L. A. Lyon, *ACS Appl. Mater. Interfaces*, 2009, **1**, 2747–2754.
22 A. B. South and L. A. Lyon, *Angew. Chem., Int. Ed.*, 2010, **49**, 767–771.
23 J. C. Gaulding, M. W. Spears and L. A. Lyon, *Polym. Chem.*, 2013, **4**, 4890–4896.
24 Z. Y. Meng, M. H. Smith and L. A. Lyon, *Colloid Polym. Sci.*, 2009, **287**, 277–285.
25 S. Saxena, M. W. Spears Jr, H. Yoshida, J. C. Gaulding, A. J. Garcia and L. A. Lyon, *Soft Matter*, 2014, **10**, 1356–1364.
26 D. E. Discher, P. Janmey and Y. L. Wang, *Science*, 2005, **310**, 1139–1143.
27 W. L. Murphy, T. C. McDevitt and A. J. Engler, *Nat. Mater.*, 2014, **13**, 547–557.
28 J. Barth, M. Buback, P. Hesse and T. Sergeeva, *Macromolecules*, 2010, **43**, 4023–4031.
29 L. M. Gu, S. P. Zhu, A. N. Hrymak and R. H. Pelton, *Macromol. Rapid Commun.*, 2001, **22**, 212–214.
30 T. Junkers and C. Barner-Kowollik, *J. Polym. Sci., Part A: Polym. Chem.*, 2008, **46**, 7585–7605.